



HAL
open science

**Grain-size reduction mechanisms and
rheological consequences in
high-temperature gabbro mylonites of Hidaka, Japan**

Hugues Raimbourg, Tsuyoshi Toyoshima, Yuta Harima, Gaku Kimura

► **To cite this version:**

Hugues Raimbourg, Tsuyoshi Toyoshima, Yuta Harima, Gaku Kimura. Grain-size reduction mechanisms and rheological consequences in high-temperature gabbro mylonites of Hidaka, Japan. *Earth and Planetary Science Letters*, 2008, 267 (3-4), pp.637-653. 10.1016/j.epsl.2007.12.012 . insu-00756068

HAL Id: insu-00756068

<https://insu.hal.science/insu-00756068>

Submitted on 22 Nov 2012

HAL is a multi-disciplinary open access archive for the deposit and dissemination of scientific research documents, whether they are published or not. The documents may come from teaching and research institutions in France or abroad, or from public or private research centers.

L'archive ouverte pluridisciplinaire **HAL**, est destinée au dépôt et à la diffusion de documents scientifiques de niveau recherche, publiés ou non, émanant des établissements d'enseignement et de recherche français ou étrangers, des laboratoires publics ou privés.

Grain size reduction mechanisms and rheological consequences in high-temperature gabbro mylonites of Hidaka, Japan

Hugues Raimbourg^a, Tsuyoshi Toyoshima^b, Yuta Harima^b, Gaku Kimura^a

(a) Department of Earth and Planetary Science, Faculty of Science, University of Tokyo,

Japan

(b) Department of Geology, Faculty of Science, University of Niigata, Japan

Corresponding Author:

Hugues Raimbourg, Dpt. Earth Planet. Science, Faculty of Science Bld #1 room 740,

The University of Tokyo, 7-3-1 Hongo, Bunkyo-ku, Tokyo 113-0033, Japan

Tel: +81-3-5841-4033

Email: hraimbou@eps.s.u-tokyo.ac.jp

Abstract

The study of microstructures and crystallographic fabrics in a granulite-facies shear zone of the Hidaka Metamorphic Belt showed that the strong shearing localized within the mylonite resulted in the asymmetrical elongation of the inherited orthopyroxene porphyroclasts and the generation of fine-grained plagioclase and orthopyroxene layers

as asymmetric tails of orthopyroxene porphyroclasts. The orthopyroxene porphyroclasts and the coarse plagioclase matrix surrounding them have a strong crystallographic preferred orientation acquired through deformation by dislocation creep. In contrast, the small orthopyroxene and plagioclase grains located in the tails have equant shapes and random fabric that are interpreted as the result of deformation by grain-boundary sliding. The small orthopyroxene grains are generated on the sheared rims of the orthopyroxene porphyroclasts by subgrain rotation, inheriting the orientation of the porphyroclasts before deforming by GBS and losing this fabric. Additional mechanism of grain-size reduction is the disruption of orthopyroxene porphyroclasts by synthetic shear zones localized on clinopyroxene exsolutions. The switch in deformation mechanism from dislocation creep to GBS, associated with the grain size reduction, yielded estimates of deviatoric stress one order smaller than lithostatic pressure. Besides, such rheological evolution attests of the mechanical softening during deformation, which contributed to the localization of the strain within the mylonite.

Keywords: EBSD, grain-size reduction, mylonite, pyroxene, grain-boundary sliding, dislocation creep

1-Introduction

The localization of ductile deformation within highly strained shear zones cutting through virtually undeformed rocks is a common feature that attests to the very heterogeneous character of viscous deformation. Crustal-scale shear zones, which can accommodate a large amount of strain, strongly contribute to the overall dynamics of the lithosphere, enabling for example lithospheric thinning along detachments in postcollisional extension (Coney, 1980; Jolivet and Patriat, 1999; Lister et al., 1984). Moreover, the mechanical description of the lower crust, whose “low” strength is much discussed (Jackson, 2002), cannot be described only by simple mineralic flow laws, but must also incorporate the large rheological variations associated with the formation of ductile shear zones.

Strain softening, i.e. weakening of the rocks undergoing deformation, is responsible for the localization of the ductile deformation in shear zones (Drury et al., 1991; Handy, 1989; Jin et al., 1998; Poirier, 1980; White et al., 1980). The relative abundance of fluids within deforming domains is one factor contributing to mechanical weakening, as “wet” minerals are more deformable than “dry” ones, irrespectively of deformation mechanism (e.g. (Dimanov et al., 2003; Rybacki and Dresen, 2000)). Another characteristic feature of shear zones is the relative small grain size with respect to host rock. The formation of

smaller grains within the deforming domains may result from the deformation itself (Karato et al., 1986; Karato et al., 1980; Post, 1977) or from recrystallizations associated with metamorphic reactions (Rubie, 1983; Rubie, 1990). But in many cases all these processes occurred concurrently, making often difficult to reconstruct the genesis of the shear zone.

In this paper we analyze a granulite-facies mylonite of the Hidaka Metamorphic Belt, on Hokkaido, Japan. The main interest of this shear zone is that small recrystallized minerals are all anhydrous and have a very similar composition to inherited porphyroclasts, therefore potentially limiting the role of water and metamorphic reactions in the mylonitization process. Such settings enable us to study the deformation-related grain size reduction and rheology variations as strain accumulates, for a given material with roughly constant composition and water content.

For this purpose, we made extensive use of electron-backscattered diffraction analysis (EBSD) on orthopyroxene and plagioclase grains, the two main constituents of the shear zones. Such fabrics analysis unravels two distinct processes concomitantly leading to grain size reduction. The difference in the crystal-preferred orientations (CPO) between the large grain and small grain fractions of both orthopyroxene and plagioclase evidences a change in deformation mechanisms, which in turn shows the rheological

softening associated with deformation. We finally use the rheological transition to get estimates on the stress and strain rate active during deformation.

2-Geological settings

The Hidaka metamorphic belt represents a deep crustal section of a Tertiary magmatic arc in the central part of Hokkaido (Komatsu et al., 1983; Komatsu et al., 1989), which consists of Cretaceous to Paleogene accretionary complexes and fore-arc basin sediments (Kiminami et al., 1986; Kiyokawa, 1992; Nanayama, 1992; Ueda, 2006). The Hidaka metamorphic belt is bounded on the west by the Poroshiri Ophiolite Zone (Western Zone) in the north and by the late Cretaceous accretionary complex in the south (Fig. 1). The boundary is a large basal fault (Hidaka Main Thrust) of the metamorphic belt, associated with a N-S trending well-developed mylonite zone (Arita et al., 1978; Hashimoto, 1975; Hashimoto, 1976; Komatsu, 1980; Komatsu et al., 1979; Miyashita and Maeda, 1978; Toyoshima, 1991). The grade of the Hidaka metamorphism decreases westward from granulite facies rocks to very low-grade metasediments of Nakanogawa Group (Osanai et al., 1991).

The regional deformation kinematics of the central part of Hokkaido including the Hidaka metamorphic belt and Poroshiri Ophiolite Zone are relatively well-defined by geodynamical reconstructions (Jolivet, 1984; Jolivet and Cadet, 1987; Jolivet et al.,

1994; Kimura, 1986; Kimura and Kusunoki, 1997; Kimura and Tamaki, 1986) as well as tectonic analyses (Arai and Miyashita, 1994; Jolivet and Miyashita, 1985; Toyoshima, 1991; Toyoshima et al., 1994; Toyoshima et al., 1997), pointing to the major dextral transpressive movement on the Hidaka Main Thrust.

Olivine gabbros and pyroxene gabbros forming the lower level of the Hidaka crustal section were exhumed through the southward transcurrent and dextral transpressive movements along its western border, the Hidaka Main Thrust (Komatsu, et al., 1989; Toyoshima, 1991; Toyoshima, et al., 1994).

The Hidaka Main Zone gabbros are mostly undeformed and preserve magmatic structures, except when crossing the Hidaka Main Thrust or in localized mylonites cutting through it.

The mylonite zone considered in this study crops out along a few tens of meters and is overlaid by a zone of undeformed gabbro. It strikes around N160 with a steep dip to the east, with a lineation striking around N015. The strong dextral deformation is clearly demonstrated by the asymmetric tails on pyroxene porphyroclasts.

3-Deformation conditions and microstructures

3-2 Mylonite microstructures

The shear zone (Fig. 2) is formed of a matrix of plagioclase embedding orthopyroxene

(opx) + minor clinopyroxene (cpx), ilmenite grains (mineral analyses in table 1).

Metamorphic foliation can be divided into two distinct kinds of layers:

-Coarse (~30-40 μm) plagioclase matrix containing large (~500 μm -1mm) opx porphyroclasts (Type 1 zones)

-Finer plagioclase (~10-20 μm) matrix containing similar large opx porphyroclasts, but also scattered small (~10 μm) grains of ilmenite and opx + minor cpx (Type 2 zones)

(Fig.2).

The inherited opx porphyroclasts often show a very elongated shape with the long axis parallel to the foliation; additionally, they have asymmetrical shapes indicating a dextral sense of shear (Toyoshima, 1991; Toyoshima, 1998).

Additional ubiquitous feature of the Type 1 zones is the presence of very thin (a few tens of μm) layers of fine-grained (10-20 μm) opx and plagioclase + minor ilmenite and cpx that extend from the asymmetrical tips of the opx porphyroclasts parallel to the foliation. Analysis of the relation between minute opx grains contained in these layers and opx porphyroclasts to which they are connected is likely to provide insights into the processes of grain-size reduction and foliation formation.

3-1 Granulite-facies metamorphism

The metamorphic paragenesis of the mylonite zone is made of plagioclase,

orthopyroxene (opx) + minor clinopyroxene (cpx), ilmenite grains. Clinopyroxene is present both as small grains and as needle-shape exsolutions within opx porphyroclasts (Fig. 2). Both opx and cpx have similar compositions in (i) porphyroclasts and exsolutions pairs and (ii) fine-grained domains. It should be noted that within the same gabbro unit, mylonitization related to retrograde hornblende crystallization have been described by (Kanagawa, 2003; Kanagawa, 2004; Kanagawa et al., submitted). The samples analyzed here do not show any amphibole, and correspond therefore to higher-grade mylonites.

Granulite-facies deformation conditions have been estimated by (Osanai, et al., 1991) as $T \approx 790-870^{\circ}\text{C}$, using the two-pyroxene thermometry (Wells, 1977; Wood and Banno, 1973), while (Toyoshima, 1993; Toyoshima et al., 2000) with the same method obtained a similar temperature interval as $T \approx 800-900^{\circ}\text{C}$. Pressure conditions estimations yielded $P \approx 6.1-7.2 \text{ kbar}$ (Osanai, et al., 1991), using the garnet-orthopyroxene-plagioclase-quartz barometer of (Newton and Perkins, 1982) in more psammitic lithologies.

4-Grain size reduction on the rims of orthopyroxene porphyroclasts

In the domains where elongated asymmetric opx porphyroclasts are connected to very

fine-grained tails, we analyzed the fabrics of opx and plagioclase using electron-backscattered diffraction (EBSD) system (Channel 5, HKL) attached to an FE-SEM microscope (JEOL JSM-7000F) available at the Department of Earth and Planetary Science, Graduate School of Science, the University of Tokyo. Lattice vectors are written as $\langle jkl \rangle$, while (jkl) refers to direction normal to plane jkl . Texture indices (J-index) were calculated with the software Salsa of EBSD Channel 5 Package, while pole figures showing isocontours of multiples of uniform distribution were generated using the David Mainprice's PF2k software.

4.1 Orthopyroxene fabrics

The opx grains we analyzed within the mylonites can roughly be divided into three subsets: the large inherited opx porphyroclasts, the small opx grains on the rims of such porphyroclasts, and the opx grains in the fine-grained tails of the porphyroclasts. In addition, for reference, we analyzed an undeformed gabbroic sample (Fig. 3 A).

4.1.1 Orthopyroxene porphyroclasts

The opx porphyroclasts, whose average length is $\sim 400\mu\text{m}$, are in average very elongated parallel to the lineation (mean aspect ratio of 8.12). In addition to this strong shape-preferred orientation, they show a strong crystallographic preferred orientation (J-index=16.2) consistent with structural framework, with the c axes concentrated

around the lineation, and the a axes perpendicular to the foliation (Fig. 3B), in agreement with prior observations by (Toyoshima, 1991). In contrast, the undeformed sample (Fig. 3A) contains large opx of similar size ($\approx 500\mu\text{m}$), but they are not elongated (mean aspect ratio 1.67) and show very scattered crystal orientations (J-index=5.5).

4.1.2 Orthopyroxene grains in the tails of porphyroclasts

Opx grains are volumetrically dominant within the tails of porphyroclasts (Fig. 3). The average grain size is $\sim 15\mu\text{m}$ and the grains have a relatively rounded shape (mean aspect ratio of 1.6). Much in contrast with the opx porphyroclasts, the small opx grains within their asymmetric tails do not seem to show any crystal-preferred orientation (J-index=3.85).

4.1.3 Orthopyroxene grains on the rims of porphyroclasts

Small opx grains were also observed on the elongated rims of the opx porphyroclasts, i.e. the face perpendicular to Z-axis, somehow connecting the two domains mentioned beforehand (Fig. 4). The domain we analyzed is located on the upper rim of a large (few mm x $500\mu\text{m}$) and elongated porphyroclast also showing a strong preferred orientation. The average grain size of this domain, $\sim 40\mu\text{m}$, and mean aspect ratio, ~ 1.5 , are relatively similar to the opx grains in the tails of the porphyroclasts. In contrast, in

spite of little scattering, this domain of small opx grains shows a relatively marked crystallographic fabric (J-index=9.4), with crystal orientations plotting close to the associated porphyroclast orientation.

4.2 Deformation mechanisms

The different opx grains analyzed in the mylonite have very distinct features depending on their size and location: (i) large porphyroclasts are very elongated and show a strong-preferred orientation (ii) small opx grains are more or less rounded and show a marked fabric on the rim of the porphyroclasts, which tend to disappear away from it.

In spite of such a difference, both fabrics are related to deformation, as they are visible only within the mylonite. Furthermore, both deformation of the opx porphyroclasts and formation/deformation of the small opx grains fraction probably correspond to the same event, as opx and cpx pairs show relatively constant compositions –and therefore T conditions– irrespective of their microstructural position, i.e. either as recrystallized small grains or as cpx exsolution within opx porphyroclasts.

4.2.1 Deformation of inherited opx porphyroclasts by dislocation creep

The strong CPO of opx porphyroclasts observed in this study is similar to fabrics reported in many natural samples (Christensen and Lundquist, 1982; Etheridge, 1975; Ishii and Sawaguchi, 2002; Kohlstedt and Van der Sande, 1973; Skemer et al., 2006).

Such a fabric is interpreted as the result of the glide on the system (100)<001> (Poirier, 1995; Raleigh, 1965; Raleigh et al., 1971): with increasing plastic strain, opx crystals deform and rotate in such a way that the glide plane (100) tends to parallel the XY foliation plane, while the Burgers vector <001> tends to parallel to the direction of shear. Such a deformation by dislocation creep, in agreement with (Toyoshima, 1991) interpretation, is consistent with the strong elongation of the opx porphyroclasts parallel to the X axis. Our comparison with undeformed samples (Fig. 3A) confirms that these features of the opx porphyroclasts within the mylonite zones (strong CPO and shape fabric) are completely acquired during deformation: opx porphyroclasts, which were rounded and randomly orientated crystals in the original rocks, progressively deformed by slip along (100)<001> system and rotated to become finally elongated grains with strongly concentrated crystal orientations.

4.2.2 Formation of the fine-grained opx fraction and associated deformation mechanism

The random CPO observed in very fine-grained opx tails of the porphyroclasts cannot be interpreted as the result of post-deformation annealing, as recrystallized opx grains located on the rims of the porphyroclasts, with a relatively similar grain size, show a marked CPO. Such random CPO is therefore the result of the deformation itself, which excludes dislocation creep as potential deformation mechanism. Possible deformation

mechanisms are diffusion creep, grain-boundary sliding or passive flow of opx grains within a more ductile matrix –see 6.1.2.

Another slightly different question regards the processes of formation of these small grains. As the small opx grains deform by a mechanism that does not generate any CPO, the CPO observed on the rims of the opx porphyroclasts is inherited –see 6.2.1.

5- Grain size reduction by disruption of the opx porphyroclasts

Another ubiquitous feature in elongated opx porphyroclasts is the presence of shear zones cutting through them with a systematic orientation (Fig. 5). Such shear zones are virtually absent of more massive opx porphyroclasts, showing that the deformation of the opx tends to weaken them.

The shear zones are constituted of small (few tens of μm) opx grains and much rarer cpx grains. Two cpx grains analyzed within the shear zone (Fig. 5) share $\langle 010 \rangle$ and $\langle 001 \rangle$ axes with adjacent opx grain. We and (Toyoshima, 1991) observed such common $\langle 010 \rangle$ and $\langle 001 \rangle$ axes between adjacent minerals in exsolutions of cpx within opx porphyroclasts, also reported in (Van Duysen et al., 1985). This exsolution geometry is related the fact that lattice parameters b and c (i.e. $\langle 010 \rangle$ and $\langle 001 \rangle$ axes) and (b,c) angle are very similar in the orthorhombic opx and monoclinic cpx; in contrast the size and orientation of a axis (i.e. $\langle 100 \rangle$ axis) differs much between opx and cpx ((Van

Duysen, et al., 1985) and references therein). As a result of this, the characteristic orientation of cpx grains with respect to adjacent opx grains within the shear zone demonstrates that such cpx crystals were formed by exsolution from a crystal of orthopyroxene, and did not nucleate as independent crystals within the shear zone. Furthermore, from the comparison of the size of cpx and opx sharing crystallographic axes, it seems unlikely that cpx crystals exsolved from the opx grain alone, but rather that exsolutions occurred within the large opx porphyroclast before it was disrupted by the shear zone. Another important observation is that we did not observe any other exsolved cpx grain in the opx porphyroclast in the vicinity of the shear zone. The localization of the shear zone seems to be controlled by the presence of cpx exsolutions, which probably act as mechanical defects to localize the formation of the shear zone.

We have further examined the kinematics of the shear zone by looking at the opx crystal orientations by EBSD. The two large opx crystals on both side of the shear zone have a very similar orientation, showing that they were a single crystal before being disjoined by the shear zone. The opx grains within the shear zone have an orientation that can be deduced from the host porphyroclast by a rotation around the Y axis of the deformation, which is the rotation axis of the macroscopic shear strain. The shear zone cutting the opx porphyroclast shows therefore a sense of movement synthetic with the shear on the

foliation plane.

We interpret these shear bands as the result of the asymmetrical “buckling” deformation of the porphyroclasts, which is possible only within the elongated grains (Fig. 6). The largest plastic deformation within the porphyroclasts localized where the crystal is weaker, i.e. where cpx is exsolved. Once a sufficient amount of strain is accumulated, a shear band develops and cuts the single elongated porphyroclast into two subgrains. Consecutive movement on the shear zone led to the rotation of the small opx grains composing it, in a movement synthetic to the main shear.

6- Discussion

6.1 Change in deformation mechanism associated with grain size reduction

6.1.1 Random fabrics in the fine-grained layers

The fine-grained layers constituting the tails of the opx porphyroclasts contain small opx showing a random fabric, but also a smaller amount of plagioclase grains. The grain size of the plagioclase in these thin tails, $\sim 10\mu\text{m}$, is much smaller than in the plagioclase matrix surrounding them, where average grain size is around $30\text{-}40\mu\text{m}$.

The analysis of the associated crystal orientations distribution unravels a large difference between the two domains of plagioclase (Fig. 7): the CPO in the fine-grained plagioclase grains within the tails of opx porphyroclasts (Fig. 7a) is much weaker than

within the coarser plagioclase grains in the matrix (Fig. 7b), as can be seen on the plot of (001) planes which are concentrated near Z-axis in Fig. 7b, but which are much more scattered and not organized consistently with structural directions in Fig. 7a.

The precise dislocation system generating the CPO of coarse-grained plagioclase domains is not clear because the CPO pattern differs slightly between analyzed domains. The most constant feature of it is the orientation of the (001) plane close to the foliation plane. (Kanagawa, 2003; Kanagawa, 2004; Kanagawa, 2006; Kanagawa, et al., submitted) and (Toyoshima, 1993), who observed the same granulite-facies mylonites, analyzed the plagioclase CPO as the result of dislocation glide on the (001) plane, with a glide direction parallel to $\langle 110 \rangle$ for the former authors and between a and b axes for the latter one.

This fabric is quite different from CPO's reported in either experimentally (Ji et al., 2005; Stunitz et al., 2003) or naturally (Ji and Mainprice, 1988; Ji et al., 1993) high temperature deformed anorthositic plagioclase samples, where plane (010) is usually parallel to foliation plane, as a result of the dislocation on $\langle 100 \rangle(010)$ or $\langle 001 \rangle(010)$ systems depending on the temperature ((Ji, et al., 2005; Stunitz, et al., 2003) and references therein). Nevertheless, (Pearce et al., 2006) has reported a plagioclase fabric with (001) parallel to Z in Archean Lewisian gneisses of NW Scotland, very similar to

what we observed in our samples. They interpreted it as the result of dominant slip on $\langle 010 \rangle (001)$ system.

In contrast to the deformation of the coarse-grained domains by dislocation creep, leading to the generation of a CPO, the weaker fabrics observed in the opx porphyroclasts tails demonstrates that the deformation of the finer-grained plagioclase is not controlled by the dislocation activity.

6.1.2 Deformation mechanism in the fine-grained layers

In a parallel fashion, coarse-grained plagioclase and opx show a marked CPO that disappears in the finer-grained domains in the tails of opx porphyroclasts, reflecting a change in deformation mechanisms from dislocation creep to mechanisms –not necessarily identical– generating a random fabric in both minerals. Several processes can account for such a random fabric: cataclastic flow, volume/grain boundary diffusion creep, grain-boundary sliding (GBS).

The opx located on the rims of the porphyroclasts can provide useful insights on the features of the deformation within the fine-grained opx fraction. The deformation within the rims of the porphyroclasts rims is still low, as is attested by the inherited CPO preserved. If we assume a formation by subgrain rotation, each of the small opx grain has originally the same crystal orientation as the porphyroclast. The rotation

vectors from this common crystal orientation to each of the actual orientations of the small grains plot near the Y-axis of the microstructure, which is also the rotation axis related to the macroscopic shear (Fig. 4). The deformation mechanism active within the fine-grained domain must therefore account for large grain rotations.

Cataclastic flow, often associated with the brittle-ductile transition (e.g. (Tullis and Yund, 1987)), can nevertheless occur at higher temperature for very high stress levels (Hadizadeh and Tullis, 1992), occurring for example with synseismic loading (Trepmann and Stöckhert, 2002). Such cataclastic flow is nevertheless unlikely in our samples, because there is no evidence of cracks or microcracks cutting through opx porphyroclasts. Furthermore, although opx porphyroclasts are clouded with cpx exsolution needles, such exsolutions are absent from small opx grains on the rims of the porphyroclasts (Fig. 2). It is therefore likely that during the formation of the opx small grains from the porphyroclast rims, the cpx exsolutions diffused out of the opx grain to crystallize the few cpx grains visible among the small opx grains, leaving homogeneous fine-grained opx. Such process of concomitant grain formation and chemical element transport is relatively incompatible with cataclastic formation, such as in (Trepmann and Stöckhert, 2002) where the intense fracturing leading to cataclastic flow crosscuts the internal chemical zonation of the garnets.

Alternative possible deformation mechanism is the passive flow of strong pyroxene grains within a softer plagioclase matrix. The rheology and deformation mechanisms of small opx and plagioclase grains are not necessarily identical: The rigid-body movement of particles of opx within a ductile matrix of plagioclase deforming by diffusion creep, would result in random fabric of both matrix and inclusions. Such a matrix-inclusion description is nevertheless not appropriate here, as in the fine-grained tails of the opx porphyroclasts, opx grains are volumetrically at least as much abundant as plagioclase grains. Therefore the fabric of the fine-grained opx fraction stems from its plastic deformation, concomitant with plagioclase deformation. Although pyroxene is often considered as a strong mineral, experiments on natural granulite samples by (Ross and Wilks, 1995), have shown that under particular conditions of high T and low stress conditions, opx is indeed softer than plagioclase.

Diffusion creep of opx, proceeding through the diffusive transfer of material along grain boundaries or within the grain volume, could be responsible of opx random CPO. It stands nevertheless at variance with the microstructure of the fine-grained tails of opx porphyroclasts, where most of the grains have a really low mean aspect ratio and no visible shape-preferred orientation. In addition, diffusion creep only does not account for the grain rotations observed on the rims of the porphyroclasts.

Naturally-deformed peridotites containing large opx porphyroclasts with fine-grained opx tails, much similar to our samples, have been analyzed by (Boullier and Gueguen, 1975), who concluded to the deformation by grain-boundary sliding (GBS) within the fine-grained opx fraction. GBS, also called sometimes superplasticity, proceeds by the relative displacement of adjacent grains along their boundary, accommodated by small variations in grain shapes by either diffusion (Ashby and Verrall, 1973) or dislocation glide (Gifkins, 1976; Hayden et al., 1972) and has been evidenced in several natural mylonites (Behrmann, 1985; Behrmann and Mainprice, 1987; Fliervoet et al., 1997).

We propose that GBS was the deformation mechanism active in the fine-grained tails of the porphyroclasts, generating the equant microstructures and random fabrics we observed (Fig. 8). As such features apply to both plagioclase and opx grains, it seems likely that the relevant deformation mechanism is two-phase GBS.

6.1.3 Stress and strain rate estimations

The transition in deformation mechanism from large plagioclase and opx grains deforming by dislocation creep to much smaller grains deforming by GBS can provide some interesting insights about the state of stress and strain rate, using experimentally-derived flow laws and the observed microstructures. The fact that the fine-grained tails of the opx porphyroclasts deform by GBS means actually that strain

rates resulting from GBS flow laws are significantly higher than strain rates from dislocation creep flow laws, both for plagioclase and opx.

Although there is no experimental flow law for GBS, theoretical modelling led (Ashby and Verrall, 1973) to derive a GBS flow law that differs from diffusion creep mainly by a constant factor ~ 7 . We can therefore compute GBS flow laws as “enhanced” diffusion creep flow laws, using the diffusion creep experimental data by (Dimanov, et al., 2003; Wang et al., 1996). Comparison of plagioclase strain rates by either GBS or dislocation creep by (Rybacki and Dresen, 2000), for $T = 850^{\circ}\text{C}$ and grain size $d = 20\mu\text{m}$, delimits a domain $\sigma \leq 35\text{MPa}$ and $\dot{\epsilon} \leq 10^{-9}\text{s}^{-1}$ where GBS is dominant and provides thereby upper bounds about the strain rate and stress conditions during deformation within the opx porphyroclasts tails (Fig. 9).

Application of the same method to the opx fraction is hindered by the absence of diffusion creep flow laws for opx. If we assume that diffusion creep of opx can be approximated using diopside flow laws by (Dimanov, et al., 2003), and use (Raleigh, et al., 1971; Ross and Nielsen, 1978) opx dislocation creep laws, GBS of opx is dominant for $\sigma \leq 15\text{MPa}$ and $\dot{\epsilon} \leq 10^{-12}\text{s}^{-1}$ (Fig. 9).

The amplitude of deviatoric stress in collision zones is little known, and recent models supporting the idea of large “overpressures” have questioned the opinion traditionally

held that deviatoric stresses are low compared to lithostatic pressure (Mancktelow, 1993; Petrini and Podladchikov, 2000; Raimbourg and Kimura, submitted). The estimation of stress in natural sample is rather difficult and always indirect. (Stöckhert et al., 1997) used the preserved foam structure of quartz to deduce very low deviatoric stress conditions during subduction and exhumation of eclogitic metapelites. Even if our results have to be taken with caution, as many approximations are made about the appropriate flow laws, the deformation conditions derived here show that the stress conditions are bounded to a few tens of MPa, therefore not significant with respect to lithostatic pressure conditions of 600MPa.

6.2 Microstructure evolution and foliation formation processes

6.2.1 Grain size reduction mechanisms

In the mylonite studied here, two processes were active to reduce the grain size -the formation of shear zones cutting through porphyroclasts and the generation of small grains on their rims- leading to the rheological evolution and the weakening of the rock. The evolution of the CPO of the small opx grains, from a preferred orientation similar to the elongated opx porphyroclasts when located on their rims to a random fabric when located far from them, shows that such small grains are generated on the rims of the porphyroclasts and inherited their CPO, before this fabric was erased by their

subsequent deformation.

One possible mechanism for CPO inheritance is the formation of new small grains on the rims of deformed opx porphyroclasts by subgrain rotation. Such process implies the organization of dislocation into walls separating slightly misorientated pyroxene domains. Phase contrast images have enabled us to observe dislocation walls separating lamellae orientated perpendicular to the long axis of elongated opx porphyroclasts (Fig 10). Misorientation angles across subgrain boundaries are around 1 or 2 degrees, while misorientation axes plot close to the crystal $\langle 010 \rangle$ axis, which is the rotation axis associated with dislocation glide on system $(100)\langle 001 \rangle$. The misorientation rate along the long axis of the opx porphyroclast is 10 times higher than in the perpendicular direction, due to the formation of misorientated lamellae. In addition to long-axis perpendicular dislocation walls, subgrains are completed as additional boundaries, roughly parallel to $\langle 001 \rangle$, develop (Fig 11). It should be noted in this example that subgrain boundary merges into the boundary of a small cpx grain exsolved within the opx porphyroclast, pointing to the role of exsolution as defects localizing the deformation such as argued in section 5.

Alternative possible mechanism leading to CPO inheritance is nucleation and growth of new grains controlled by the porphyroclast crystal orientation (Jiang et al., 2000). Such

process probably may partly contribute to small opx grains formation in our samples, but it stands slightly at variance with the fact that small grains are not generated all along the porphyroclasts surface, but preferentially along their sheared rims, i.e. the side parallel to the foliation. Therefore, the generation of the small opx grains with inherited CPO probably results mainly from subgrain rotations of the rims of the opx porphyroclasts deforming by dislocation creep.

6.2.2 Mylonite formation: weakening mechanism

Strain-weakening mechanisms are a key property to the formation of mylonite zones, as it results in a strong localization of the deformation. Within the mylonites considered here, fluid flow and metamorphic reactions probably play a minor role in the strain-weakening processes, which rely mainly on deformation-controlled grain-size variations.

The fine-grained tails of the opx porphyroclasts developed along with strain within the mylonite. The switch in deformation mechanism of both opx and plagioclase associated with grain size reduction, from grain-size independent dislocation creep to grain-size dependent GBS, implies that the fine-grained tails of the porphyroclasts are mechanically weaker than the opx porphyroclasts or the coarser-grained plagioclase matrix. The interconnection of the fine-grained tails between the scattered

porphyroclasts creates soft surfaces which accommodate much more deformation than surrounding matrix and therefore weaken the average rheology of the rock.

The deformation itself, at the origin of the generation of small opx and plagioclase grains, is therefore responsible of a rheological softening of the mylonite, contributing to the strong partitioning of the strain within it.

6.2.3 Mylonite formation: development of a foliated structure

The large strain accumulated within the mylonite often results in the development of a foliation, crosscutting any possible preexisting structure of host rock. Foliation development in metamorphic rocks can result from various process, e.g. oriented growth of grains (Stallard and Shelley, 2005a) or metamorphic segregation of minerals (Stallard et al., 2005b). In addition, the properties of the flow within the mylonite control its structural evolution. The very high viscosity of rocks and the slow deformation rates result in a very low Reynolds number (Batchelor, 1967) flows, i.e. laminar flows, reflected in the foliated structure of the mylonite. Another important factor controlling the flow properties is the mechanical contrast between minerals or layers.

One element defining the mylonitic foliation in our samples is the fine-grained tails of the opx porphyroclasts. The length of these tails is variable, from a few microns to

several mm-long domains connecting several opx porphyroclasts, while their width is at most a few tens of microns. The formation of such tails (Fig. 12) requires that the small opx grains generated on top of opx porphyroclasts are not dispersed within the plagioclase matrix, but deform into elongated domains parallel to the mylonite foliation. Such a feature is probably related to the rheological contrast between the weak fine-grained domains and the stronger plagioclase matrix. It is interesting to note that in contrast to this behaviour, within the much finer-grained plagioclase matrix layers (Fig. 12), the opx small grains are dispersed within the matrix, as a result of the smaller rheological contrast between opx and plagioclase grains.

The weak rheology of the tails of the opx may also be responsible for the formation of the small plagioclase grains that can be found within it. The stress concentration at the tips of the weakened domains, in a fashion much similar to crack tips, may provide the conditions for the recrystallization of small plagioclase grains, and further contribute to the propagation of the mechanically soft tails of the porphyroclasts.

7- Conclusions

The analysis of microstructures and crystal orientation distribution within high-grade mylonites of the Hidaka Metamorphic Belt showed the importance of grain size reduction processes affecting inherited opx porphyroclasts. As strain accumulated

within opx porphyroclasts, small opx grains formed by subgrain rotation on their rims and in shear zones cutting through them. Opx grains present in fine-grained (10-20 μ m) layers deformed by grain-size dependent GBS, in contrast to the coarser-grains deforming by grain-size independent dislocation creep. This switch in deformation mechanisms attests of the mechanical softening associated with the grain size reduction. The fine-grained domains, including both small opx and plagioclase grains, developed as very thin and long tails of the inherited opx porphyroclasts, creating an interconnected network of mechanically weak surfaces, which contributed to the partitioning of all deformation within the mylonite.

Figures

Figure 1: Simplified geological map of the Hidaka Metamorphic Belt from [Toyoshima, et al., 1994], and location of the mylonite zone studied (star).

Figure 2: Microstructures of the mylonite zone. All images in the XZ plane, with dextral shear horizontal. (A) Thin section scan, (B) and (D) optical microscope images, (C) EPMA map of the distribution of Ca. The mylonite is constituted of an alternance of fine grained and coarse-grained plagioclase domains, asymmetrically elongated opx porphyroclasts with fine-grained tails. The detailed compositional mapping in Ca (C) shows the abundance of cpx exsolutions within opx porphyroclasts, and the presence of small grains of exsolution-free opx, cpx and ilmenite on the rim of the porphyroclasts.

Figure 3: (A) Opx crystal orientation in undeformed samples, corresponding to the magmatic texture. Opx porphyroclasts crystals are randomly orientated and opx grains have a rounded shape. (B) and (B') Analyses of opx in mylonite samples. (B) Inherited opx porphyroclasts developed a strong fabric, related to the $\langle 001 \rangle (100)$ dislocation system activity. Most porphyroclasts are elongated parallel to the lineation. (B') In

contrast, small grains of opx in the tails of porphyroclasts, show a relatively rounded shape and a random CPO. All pole figures were drawn using David Mainprice's Pf2k software with equal area and lower hemisphere projection. Contours and shading correspond to multiples of uniform distribution. Maximum density value normalized by uniform distribution is indicated on top of the gray scale and corresponds to the black square on the plot. N is the number of analyzed grains and J is the J-index value, calculated from the orientation distribution function computed using the software Salsa in Channel 5 package.

Figure 4: (A) SEM-forescatter image and (B) CPO of small opx grains domain on the sheared rim of opx porphyroclasts. Small opx grains have a strong CPO which is close to the porphyroclast crystal orientation. Same conventions as Fig. 4 (C) Rotations vectors, calculated between actual orientation of each grain and porphyroclast orientation –considered as the original orientation of each grain– plot near the Y axis of the deformation, i.e. rotation axis associated with the macroscopic shear.

Figure 5: (A) EBSD map of an elongated opx porphyroclast cut by a shear zone containing mainly opx grains and few cpx grains. (B) Diffraction patterns (raw and

interpreted patterns) of two adjacent cpx and opx grains within the shear zone (forescatter image with the one opx and three cpx contours underlined), showing common (100) planes. (C) Crystal orientations of opx porphyroclast on both sides of the shear zone (crosses locations on (B) image) and of opx grains within the shear zone.

Figure 6: Model of shear zone formation in porphyroclasts: (A) Sheared opx porphyroclasts are elongated through the movement of dislocations. (B) Once sufficiently thinned, they buckle and fold preferentially in their weaker sections, i.e. where large cpx exsolutions are present. (C) Eventually, the folded region breaks into a microshear zone composed of small opx grains, which start deforming by GBS and rotate clockwise with respect to their original orientation, as a result of a synthetic deformation on the microshear zone.

Figure 7: (A) SEM fore-scatter image of a fine-grained layer within coarse-grained plagioclase matrix. (B) EBSD map of coarse-grained plagioclase matrix. Plagioclase crystals within the fine-grained layers show a much weaker orientation than matrix grains, as can be seen for example in the distribution of poles to (001) planes, rather randomly distributed in the fine-grained layers (A) and concentrated perpendicular to

the foliation for matrix grains (B). See Fig. 3 for details of projections.

Figure 8: Model of opx deformation: Opx porphyroclasts are deformed and elongated by dislocation creep. On the sheared rims of these porphyroclasts, small opx grains are formed by subgrain rotation and inherit a strong crystal preferred orientation. This small grain deform by GBS, which eventually erase the inherited fabric, so that in the tail far from the porphyroclasts the opx have a random fabric.

Figure 9: Stress estimation: within the fine-grained tails of opx porphyroclasts, GBS must be dominant over dislocation creep for both opx and plagioclase, defining upper bounds on stress and strain rates (green domain=admissible range). In particular, stress conditions are limited to a few tens of MPa, i.e. much lower than lithostatic pressure of 600MPa. Temperature and grain size are fixed as 850°C and 20µm, respectively. GBS flow laws are defined from diffusion creep flow laws using an enhancing factor ~ 7 from GBS model by [Ashby and Verrall, 1973].

Figure 10: Dislocation walls and subgrain formation: (A) Forescatter image highlights the slight misorientation between adjacent lamellae within the opx porphyroclasts. (B)

Misorientation angle (diamonds) along the upper trail of (A) with respect to the first point 0, showing a mean rotation rate of around 0.25 degree per micron in the direction parallel to porphyroclast long axis, 10 times higher than the rotation rate in the perpendicular direction assessed along the (a,a'), (b,b') and (c,c') pairs. Rotation rates between adjacent points (rectangles) along the same trail show very high values at boundaries between lamellae, corresponding to dislocation walls. (C) Misorientation axes in the porphyroclast crystal framework: Along the two trails parallel to porphyroclast long axis, most misorientation axes plot close to pyroxene $\langle 010 \rangle$ axis. (D) Porphyroclast orientations in the structural framework. $\langle 100 \rangle$ and $\langle 001 \rangle$ axes are much more scattered than $\langle 010 \rangle$ axis, as a result of dislocation-related rotation around $\langle 010 \rangle$ axis.

Figure 11: Subgrain formation in opx porphyroclasts: (A) Subgrains, seen as contrasted domains on the rim of opx porphyroclasts, are delimited by boundaries either perpendicular or parallel to $\langle 001 \rangle$ axis of porphyroclasts. Locally subgrain boundary merges into cpx exsolution boundary. (B) EBSD map of opx crystal orientation, showing that subgrain orientation is hardly distinguishable from surrounding opx porphyroclast.

Figure 12: Model of foliation development: (A) As the fine-grained zone is weaker than surrounding matrix, stresses are concentrated at both of its tips. Within this zone of high stresses, small grains of plagioclase are dynamically recrystallized. In parallel, small opx grains are generated on the rims of the opx porphyroclasts. Both plagio and opx grains are transported through the deformation, giving rise to the development of the fine-grained layers, to the right in layers on top of the porphyroclasts, to the left in the bottom layer. (B) Because of their weakness, in a fashion similar to cracks, weak layers tend to connect to each other. After sufficient strain, the average rheology of the mylonite is controlled by a continuous network of weak fine-grained layers.

Table 1: EPMA analyses of representative minerals. *Italic*: minerals in the fine-grained tails of opx porphyroclasts. Plain: opx porphyroclasts and coarse-grained plagioclase matrix.

References

Arai, T., Miyashita, S., 1994. Shear deformation and metamorphism of the Poroshiri

- Ophiolite in the Shunbetsu River region, the Hidaka belt, Hokkaido, Japan. *Jour. Geol. Soc. Japan* 100, 162-176.
- Arita, K., Mori, M., Ogura, K., Motoyoshi, Y., 1978. The metamorphic rocks and migmatites of the southern part of the Hidaka Metamorphic Belt. *Assoc. Geol. Collabor. Japan Monograph* 21, 27-41.
- Ashby, M.F., Verrall, R.A., 1973. Diffusion-accommodated flow and superplasticity. *Acta Metallurgica* 21, 149-163.
- Batchelor, G.K., 1967. *An introduction to fluid dynamics*, Cambridge University Press, New York.
- Behrmann, J.H., 1985. Crystal plasticity and superplasticity in quartzite: a natural example. *Tectonophysics* 115, 101-129.
- Behrmann, J.H., Mainprice, D., 1987. Deformation mechanisms in a high-temperature quartz-feldspar mylonite: evidence for superplastic flow in the lower continental crust. *Tectonophysics* 140, 297-305.
- Boullier, A.M., Gueguen, Y., 1975. SP-Mylonites: Origin of some mylonites by superplastic flow. *Contrib. Mineral. Petr.* 50, 93-104.
- Christensen, N.I., Lundquist, S.M., 1982. Pyroxene orientation within the upper mantle. *GSA Bull.* 93, 279-288.

- Coney, P.J., 1980. Cordilleran metamorphic core complexes, in: Crittenden, M.D., P.J. Coney, G.H. Davis, (Eds), Cordilleran Metamorphic Core Complexes, GSA Memoir 153, Boulder, pp. 7-34.
- Dimanov, A., Lavie, M.P., Dresen, G., Ingrin, J., Jaoul, O., 2003. Creep of polycrystalline anorthite and diopside. *J. Geophys. Res.-Sol. Ea.* 108, doi:10.1029/2002JB001815.
- Drury, M.R., Vissers, R.L.M., Van der Wal, D., Hoogerduijn Strating, E.H., 1991. Shear localization in upper mantle peridotites. *Pure Appl. Geophys.* 137, 439-460.
- Etheridge, M.A., 1975. Deformation and recrystallization of orthopyroxene from the Giles Complex, central Australia. *Tectonophysics* 25, 87-114.
- Fliervoet, T.F., White, S.H., Drury, M.R., 1997. Evidence for dominant grain-boundary sliding deformation in greenschist- and amphibolite-grade polymineralic ultramylonites from the Redbank Deformed Zone, Central Australia. *J. Struct. Geol.* 19, 1495-1520.
- Gifkins, R.C., 1976. Grain boundary sliding and its accommodation during creep and superplasticity. *Metall. Trans.* 7A, 1225-1232.
- Hadizadeh, J., Tullis, J., 1992. Cataclastic flow and semi-brittle deformation of anorthosite. *J. Struct. Geol.* 14, 57-63.
- Handy, M.R., 1989. Deformation regimes and rheological evolution of fault zone in the

- lithosphere: the effects of pressure, temperature, grain-size and time.
Tectonophysics 163, 119-152.
- Hashimoto, S., 1975. The basic plutonic rocks of the Hidaka Metamorphic Belt, Hokkaido.
Part I. J. Fac. Sci. Hokkaido Univ., Ser. IV 16, 367-420.
- Hashimoto, S., 1976. Structural significance of the Western Zone of the Hidaka
Metamorphic Belt. Rept. Geol. Min. Niigata Univ. 4, 409-414.
- Hayden, H.W., Floreen, S., Goodell, P.D., 1972. the deformation mechanism of
superplasticity. Metall. Trans. 3, 833-842.
- Ishii, K., Sawaguchi, T., 2002. Lattice- and shape-preferred orientation of orthopyroxene
porphyroclasts in peridotites: an application of two-dimensional numerical modeling.
J. Struct. Geol. 24, 517-530.
- Jackson, J., 2002. Strength of the continental lithosphere: time to abandon the jelly
sandwich? GSA Today 12, 4-10.
- Ji, S., Mainprice, D., 1988. Natural deformation fabrics of plagioclase: implications for slip
systems and seismic anisotropy. Tectonophysics 147, 145-163.
- Ji, S., Rybacki, E., Wirth, R., Jiang, Z., Xia, B., 2005. Mechanical and microstructural
characterization of calcium aluminosilicate (CAS) and SiO₂/CAS composites
deformed at high temperature and high pressure. J. Eur. Ceram. Soc. 25, 301-311.

- Ji, S., Salisbury, M.H., Hanmer, S., 1993. Petrofabric, P-wave anisotropy and seismic reflectivity of high-grade tectonites. *Tectonophysics* 222, 195-226.
- Jiang, Z., Prior, D.J., Wheeler, J., 2000. Albite crystallographic preferred orientation and grain misorientation distribution in a low-grade mylonite: implications for granular flow. *J. Struct. Geol.* 22, 1663-1674.
- Jin, D., Karato, S.-I., Obata, M., 1998. Mechanisms of shear localization in the continental lithosphere: inference from the deformation microstructures of peridotites from the Ivrea zone, northwestern Italy. *J. Struct. Geol.* 20, 195-209.
- Jolivet, L., 1984. The Structure Of Meta-Ophiolitic Zone (Hokkaido, Japan) - A Right-Lateral Strike-Slip Movement. *Comptes Rendus Academie des Sciences Serie II* 298, 229-234.
- Jolivet, L., Cadet, J.P., 1987. Tectonic Evolution Of The Hokkaido Central Belt - A Model. *Bull. Soc. Geol. de France* 3, 487-497.
- Jolivet, L., Miyashita, S., 1985. The Hidaka Shear Zone (Hokkaido, Japan) - Genesis During A Right-Lateral Strike-Slip Movement. *Tectonics* 4, 289-302.
- Jolivet, L., Patriat, M., 1999. Ductile extension and the formation of the Aegean sea, in: Durand, B., L. Jolivet, F. Horvath, M. Séranne, (Eds), *The Mediterranean basins: Tertiary extension within the Alpine Orogen*, *Geol. Soc. Lond.* 156, pp. 427-456.

Jolivet, L., Tamaki, K., Fournier, M., 1994. Japan Sea, Opening History And Mechanism - A

Synthesis. *J. Geophys. Res.* 99, 22237-22259.

Kanagawa, K., 2003. Rheology of lower crustal fault rocks: an example of the Pankenushi

gabbro mylonite, Earth and Planetary Science Joint Meeting, Abstr. J063-019

Kanagawa, K., 2004. Superplastic flow of reaction products in mylonites, Japan Earth and

Planetary Science Joint Meeting, Abstr. J078-017

Kanagawa, K., 2006. Dynamic recrystallization and CPO of plagioclase: examples of mafic

mylonites from the Hidaka metamorphic belt and Kohistan Arc, Japan Geoscience

Union Meeting, Abstr. I142-002

Kanagawa, K., Shimano, H., Hiroi, Y., submitted. Mylonitic deformation of gabbro in the

lower crust: an example of the Pankenushi gabbro in the Hidaka metamorphic belt

of central Hokkaido, Japan. *J. Struct. Geol.*

Karato, S., Paterson, M.S., Fitzgerald, J.D., 1986. Rheology of synthetic olivine aggregates:

influence of grain size and water. *J. Geophys. Res.* 91, 8151-8176.

Karato, S., Toriumi, M., Fujii, T., 1980. Dynamic recrystallization of olivine single crystals

during high-temperature creep. *Geophys. Res. Lett.* 7, 649-652.

Kiminami, K., Miyashita, S., Kimura, G., Takika, J., Iwata, K., Sakai, A., Yoshida, A., Kato,

Y., Watanabe, Y., Ezaki, Y., Kontani, Y., Katsushima, T., 1986. Mesozoic rocks in the

- Hidaka belt-Hidaka Supergroup, Assoc. Geol. Collabor. Japan Monograph 31, pp. 137-155.
- Kimura, G., 1986. Oblique Subduction And Collision - Fore-Arc Tectonics Of The Kuril Arc. *Geology* 14, 404-407.
- Kimura, G., Kusunoki, K., 1997. The Hidaka Orogeny and tectonics of arc-arc junction. *Mem. Geol. Soc. Japan* 47, 295-305.
- Kimura, G., Tamaki, K., 1986. Collision, Rotation, And Back-Arc Spreading In The Region Of The Okhotsk And Japan Seas. *Tectonics* 5, 389-401.
- Kiyokawa, S., 1992. Geology of the Idonnappu Belt, Central Hokkaido, Japan: evolution of a Cretaceous accretionary complex. *Tectonics* 11, 1180-1206.
- Kohlstedt, D.L., Van der Sande, J.B., 1973. Transmission electron microscopy investigation of the defect microstructure of four natural orthopyroxenes. *Contrib. Mineral. Petr.* 42, 169-180.
- Komatsu, M., 1980. Garnet-granulite and garnet-amphibolite zone of the Hidaka Metamorphic Belt, 87th Ann. Meet. Geol. Soc. Japan, Abstr. 294
- Komatsu, M., Arita, K., Miyashita, S., Maeda, J., Motoyoshi, Y., 1979. The boundary between the Western Zone and the Main Zone of the Hidaka Metamorphic Belt, 86th Ann. Meet. Geol. Soc. Japan, Abstr. 289

Komatsu, M., Miyashita, S., Maeda, J., Osanai, Y., Toyoshima, T., 1983. Disclosing of a deepest section of continental type crust up-thrust as the final event of collision of arcs in Hokkaido, north Japan, in: Hashimoto, M., S. Uyeda, (Eds), *Accretion tectonics in the circum-Pacific regions*, TerraPub, Tokyo, pp. 149-165.

Komatsu, M., Osanai, Y., Toyoshima, T., Miyashita, S., 1989. Evolution of the Hidaka metamorphic belt, northern Japan, in: Daly, J.S., R.A. Cliff, B.W.D. Yardley, (Eds), *Evolution of metamorphic belts*, Geol. Soc. Spec. Pub. 43, pp. 487-493.

Lister, G.S., Banga, G., Feenstra, A., 1984. Metamorphic core complexes of Cordilleran type in the Cyclades, Aegean Sea, Greece. *Geology* 12, 221-225.

Mancktelow, N.S., 1993. Tectonic overpressure in competent mafic layers and the development of isolated eclogites. *J. Metamorph. Geol.* 11, 801-812.

Miyashita, S., Maeda, J., 1978. The basic plutonic and metamorphic rocks from the northern Hidaka Metamorphic Belts, Hokkaido. *Assoc. Geol. Collabor. Japan Monograph* 21, 43-60.

Nanayama, F., *Sedimentology and sedimentary petrology of the Nakanogawa Group in the Hidaka belt, central Hokkaido, Japan: Three petroprovinces identified in the Paleocene Nakanogawa Group and their geotectonic significance.*, Hokkaido University, 1992.

Newton, R.C., Perkins, D., 1982. Thermodynamic calibration of geobarometers based on the assemblage garnet-plagioclase-orthopyroxene(clinopyroxene)-quartz. *Am. Mineral.* 69, 203-222.

Osanai, Y., Komatsu, M., Owada, M., 1991. Metamorphism and granite genesis In the Hidaka Metamorphic Belt, Hokkaido, Japan. *J. Metamorp. Geol.* 9, 111-124.

Pearce, M.A., Wheeler, J., Prior, D.J., 2006. Plagioclase deformation - evidence from EBSD and chemical zoning, Gordon Research Conference: Rock Deformation, Abstr.

Petrini, K., Podladchikov, Y., 2000. Lithospheric pressure-depth relationship in compressive regions of thickened crust. *J. Metamorph. Geol.* 18, 67-77.

Poirier, J.P., 1980. Shear localization and shear instability in materials in the ductile field. *J. Struct. Geol.* 2, 135-142.

Poirier, J.P., 1995. Plastic rheology of crystals, *Mineral Physics and crystallography, a handbook of physical constants*, AGU, pp. 237-247.

Post, R.L., 1977. High-temperature creep of Mt. Burnett dunite. *Tectonophysics* 42, 75-110.

Raimbourg, H., Kimura, G., submitted. Non-lithostatic pressure in subduction zones. *EPSL*.

Raleigh, C.B., 1965. Glide mechanisms in experimentally deformed minerals. *Science* 150, 739-741.

Raleigh, C.B., Kirby, S.H., Carter, N.L., Ave Lallemand, H.G., 1971. Slip and the

- clinoenstatite transformation as competing rate processes in enstatite. *J. Geophys. Res.* 76, 4011-4022.
- Ross, J.V., Nielsen, K.C., 1978. High-temperature flow of wet polycrystalline enstatite. *Tectonophysics* 44, 233-261.
- Ross, J.V., Wilks, K.R., 1995. Effects of a third phase on the mechanical and microstructural evolution of a granulite. *Tectonophysics* 241, 303-315.
- Rubie, D., 1983. Reaction-enhanced ductility: The role of solid-solid univariant reactions in deformation of the crust and mantle. *Tectonophysics* 96, 331-352.
- Rubie, D.C., 1990. Mechanisms of reaction-enhanced deformability in minerals and rocks, in: Barber, D.J., P.G. Meredith, (Eds), *Deformation Processes in Minerals, Ceramics and Rocks*, Unwin-Hyman, London, pp. 262-295.
- Rybacki, E., Dresen, G., 2000. Dislocation and diffusion creep of synthetic anorthite aggregates. *J. Geophys. Res.* 105, 26017-26036.
- Skemer, P., Katayama, I., Karato, S., 2006. Deformation fabrics of the Cima di Gagnone peridotite massif, Central Alps, Switzerland: evidence of deformation at low temperatures in the presence of water. *Contrib. Mineral. Petr.* 152, 43-51.
- Stallard, A., Shelley, D., 2005a. The initiation and development of metamorphic foliation in the Otago Schist, Part 1: competitive oriented growth of white mica. *J. Metamorp.*

Geol. 23, 425-442.

Stallard, A., Shelley, D., Reddy, S., 2005b. The initiation and development of metamorphic foliation in the Otago Schist, Part 2: evidence from quartz grain-shape data. *J. Metamorp. Geol.* 32, 443-459.

Stöckhert, B., Massone, H.-J., Nowlan, E.U., 1997. Low differential stress during high-pressure metamorphism: The microstructural record of a metapelite from the Eclogite Zone, Tauern Window, Eastern Alps. *Lithos* 41, 103-118.

Stunitz, H., Fitzgerald, J.D., Tullis, J., 2003. Dislocation generation, slip systems, and dynamic recrystallization in experimentally deformed plagioclase single crystals. *Tectonophysics* 372, 215-233.

Toyoshima, T., 1991. Tectonic evolution of the Hidaka metamorphic belt and its implication in late Cretaceous-Middle Tertiary Tectonics of Hokkaido, Japan, *Science reports of Niigata University Series E, Geology and Mineralogy*, No. 8.

Toyoshima, T., 1993. Mylonitization in a lower crustal level granulite facies mylonites in the Hidaka metamorphic belt, Hokkaido, northern Japan, *Geol. Soc. Japan Meeting*, Abstr. 598

Toyoshima, T., 1998. Gabbro mylonite developed along a crustal-scale decollement, in: Snoke, A.W., J. Tullis, V.R. Todd, (Eds), *Fault-related Rocks: A photographic Atlas*,

Princeton University Press, pp. 426-427.

Toyoshima, T., Komatsu, M., Niizato, T., 2000. Granulite-grade gabbroic mylonites and
crustal-scale decollement in a deep crust exposed in the Hidaka metamorphic belt,
Geol. Soc. Japan Meeting, Abstr. 277

Toyoshima, T., Komatsu, M., Shimura, T., 1994. Tectonic evolution of lower crustal rocks in
an exposed magmatic arc section in the Hidaka metamorphic belt, Hokkaido,
northern Japan. *Island Arc* 3, 182-198.

Toyoshima, T., Komatsu, M., Shimura, T., 1997. Tectonics of the Hidaka metamorphic belt,
Hokkaido, northern Japan. *Mem. Geol. Soc. Japan* 47, 259-277.

Trepmann, C., Stöckhert, B., 2002. Cataclastic deformation of garnet: a record of synseismic
loading and postseismic creep. *J. Struct. Geol.* 24, 1845-1856.

Tullis, J., Yund, R.A., 1987. Transition from cataclastic flow to dislocation creep of feldspar:
Mechanisms and microstructures. *Geology* 15, 606-609.

Ueda, H., 2006. Geologic structure Cretaceous accretionary complexes in the frontal Hidaka
collision zone, Hokkaido, Japan. *J. Geol. Soc. Japan* 112, 699-717.

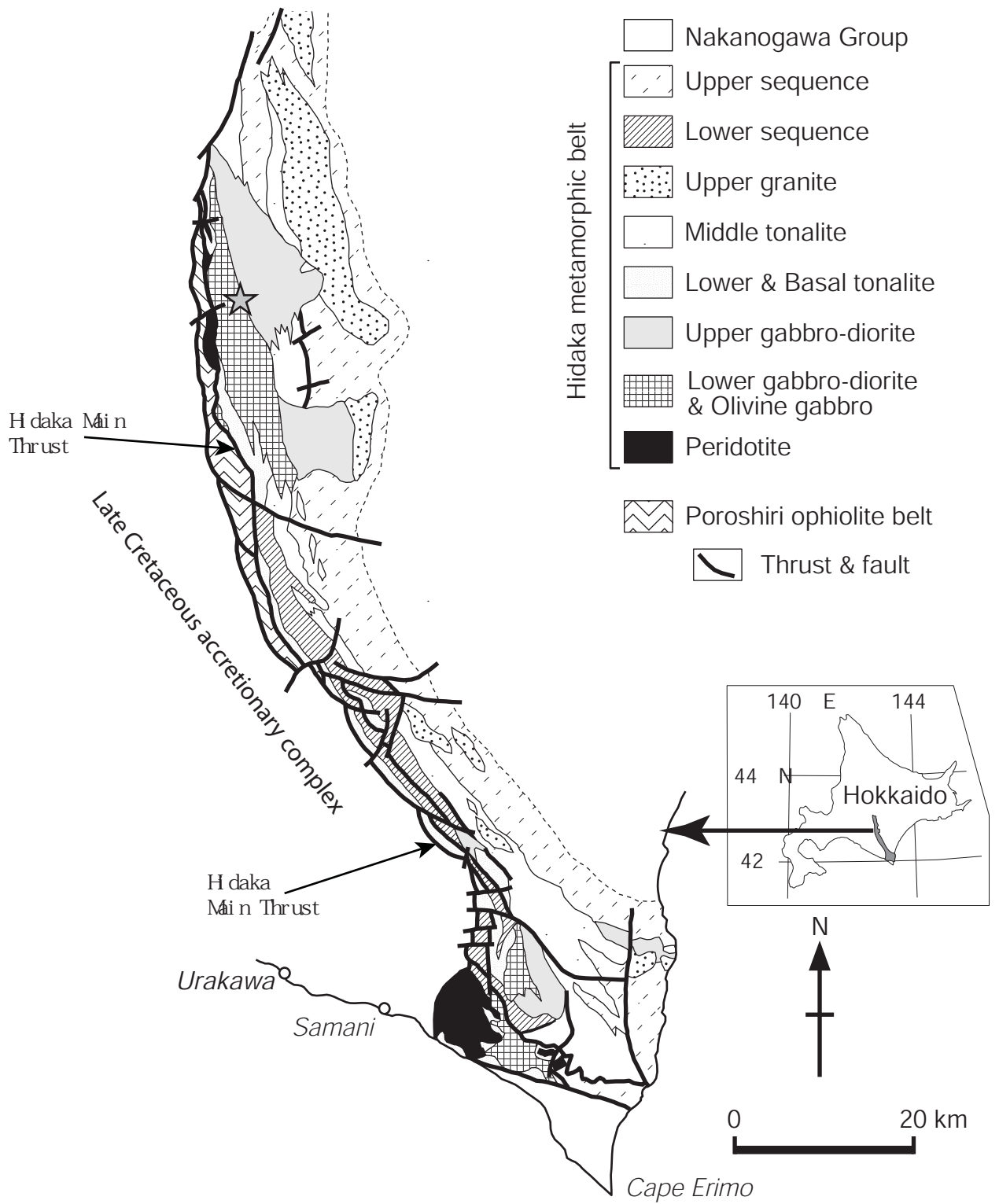
Van Duysen, J.C., Doukhan, N., Doukhan, J.C., 1985. Transmission electron microscope
study of dislocations in orthopyroxene (Mg, Fe)₂Si₂O₆. *Phys. Chem. Minerals* 12,
39-44.

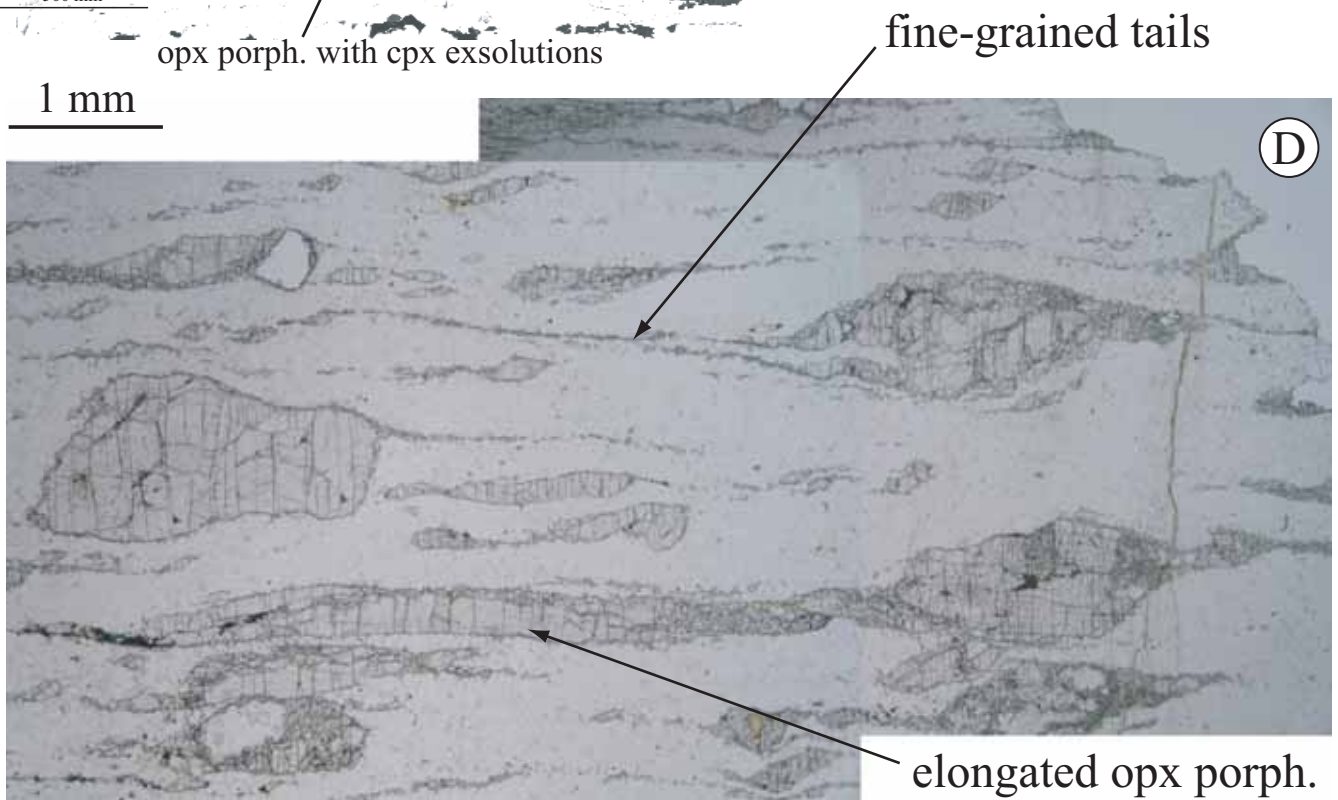
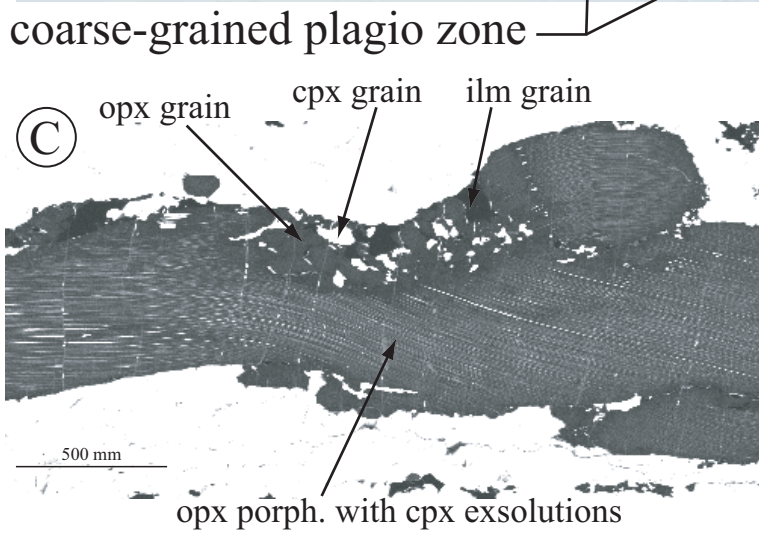
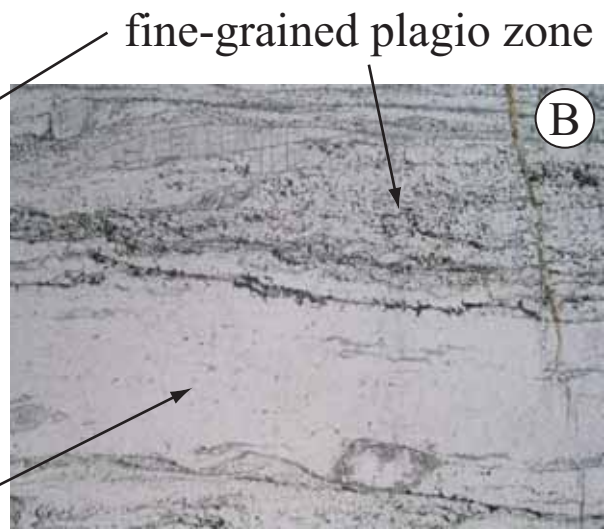
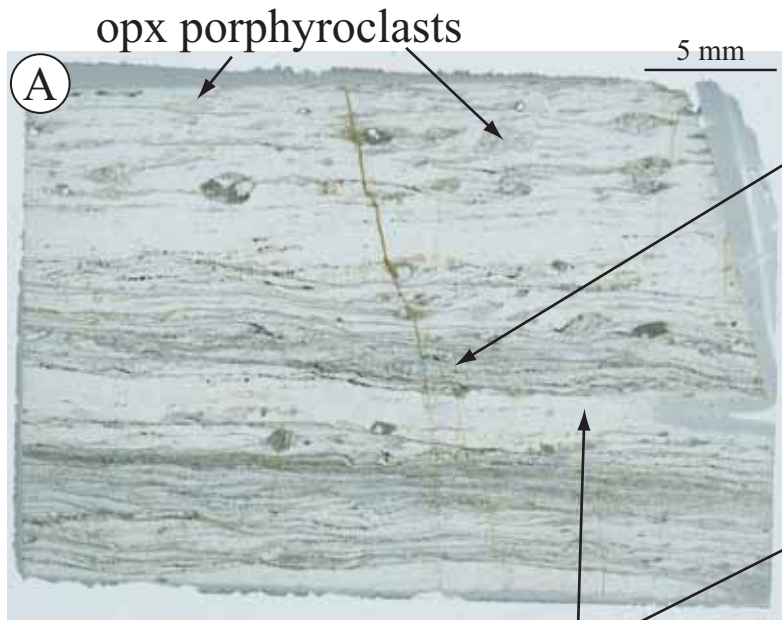
Wang, Z., Dresen, G., Wirth, R., 1996. Diffusion creep of fine-grained polycrystalline anorthite at high-temperature. *Geophys. Res. Lett.* 23, 3111-3114.

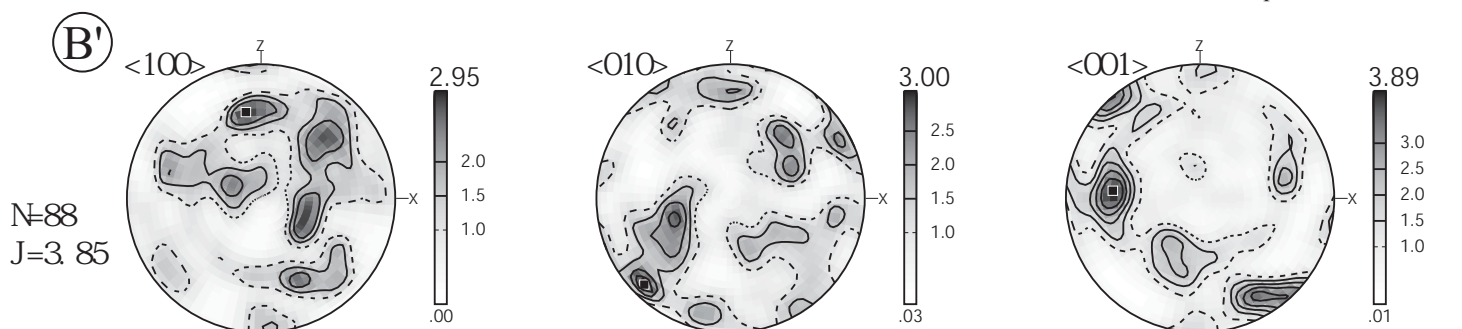
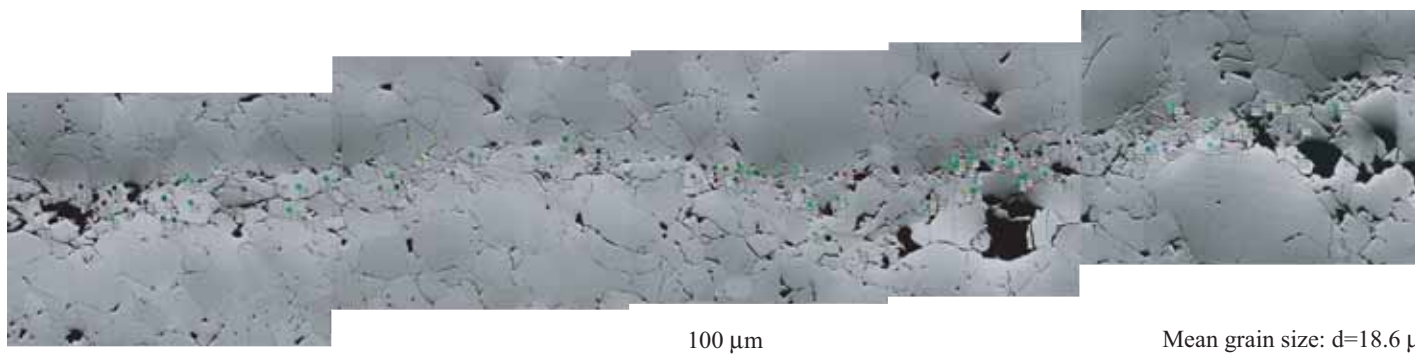
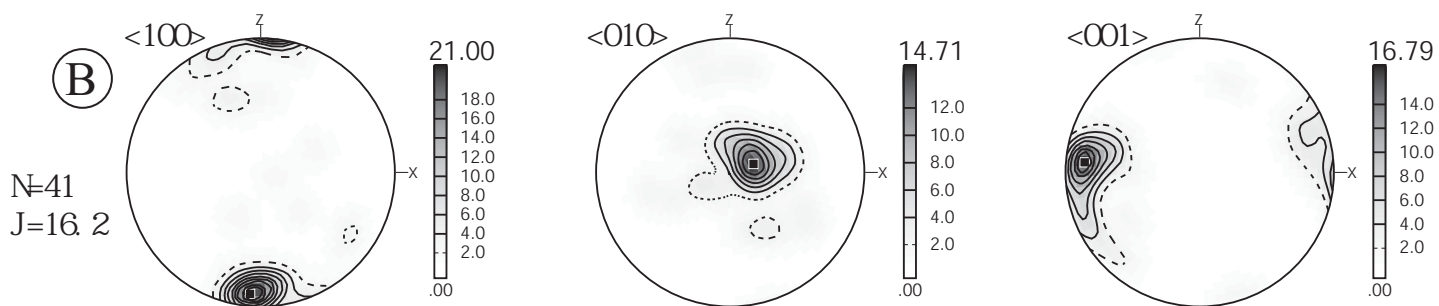
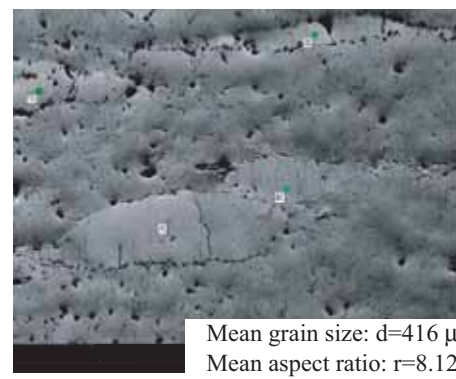
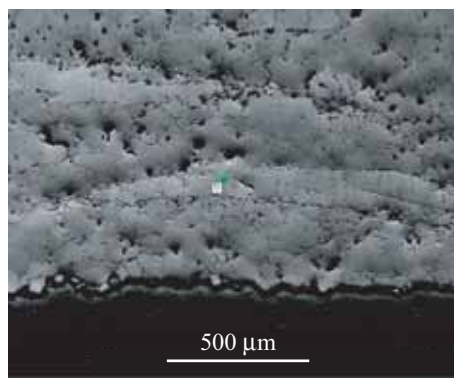
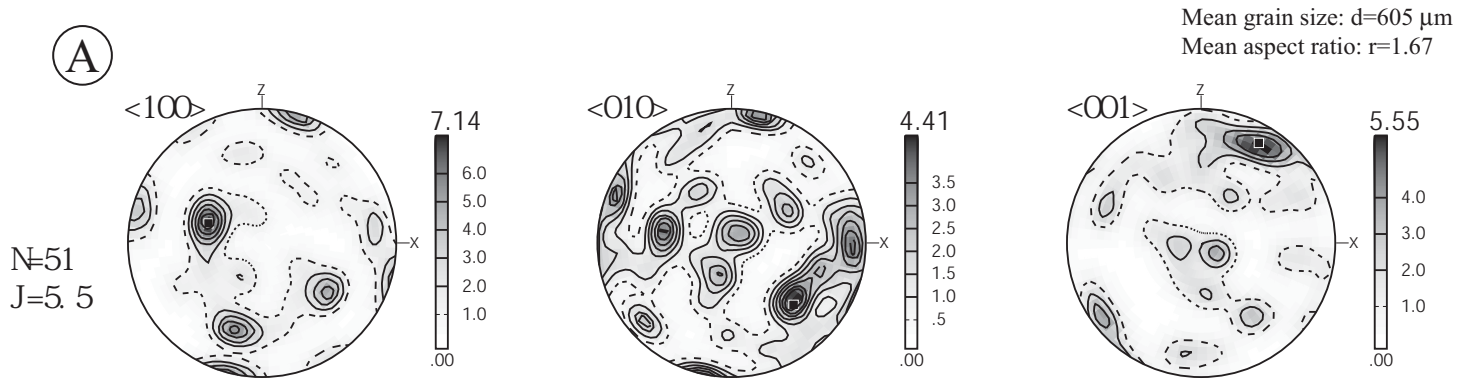
Wells, P.R.A., 1977. Pyroxene thermometry in simple and complex systems. *Contrib. Mineral. Petr.* 69, 129-139.

White, S.H., Burrows, S.E., Shaw, N.D., Humphreys, F.J., 1980. On mylonites in ductile shear zones. *J. Struct. Geol.* 2.

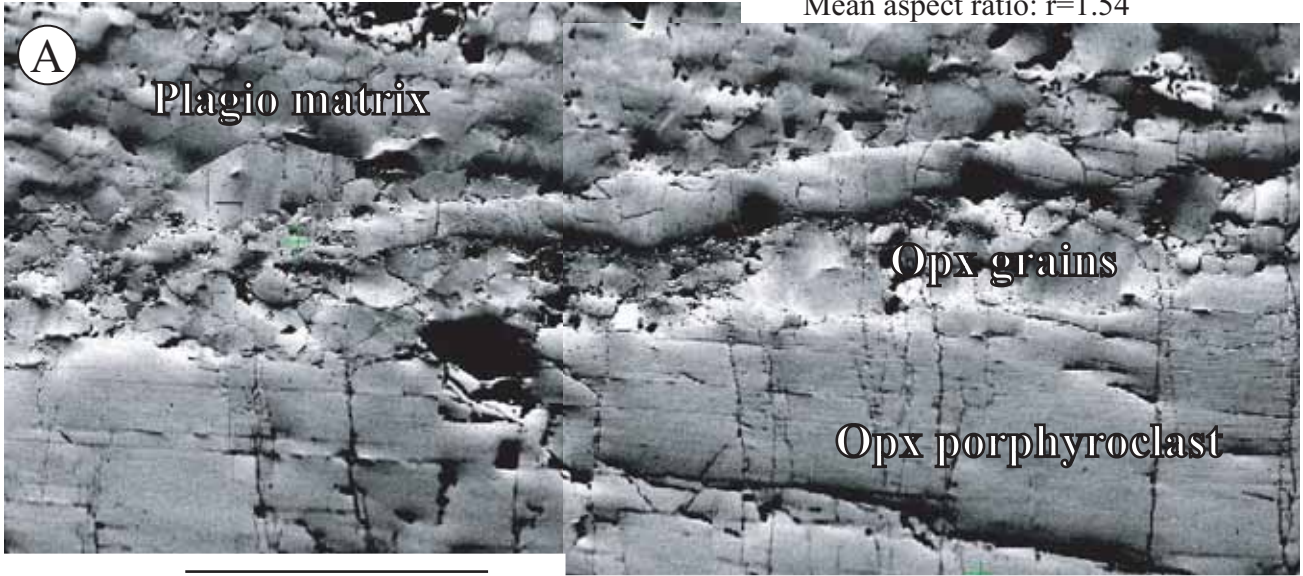
Wood, B.J., Banno, S., 1973. Garnet-orthopyroxene-clinopyroxene in simple and complex systems. *Contrib. Mineral. Petr.* 42, 109-124.



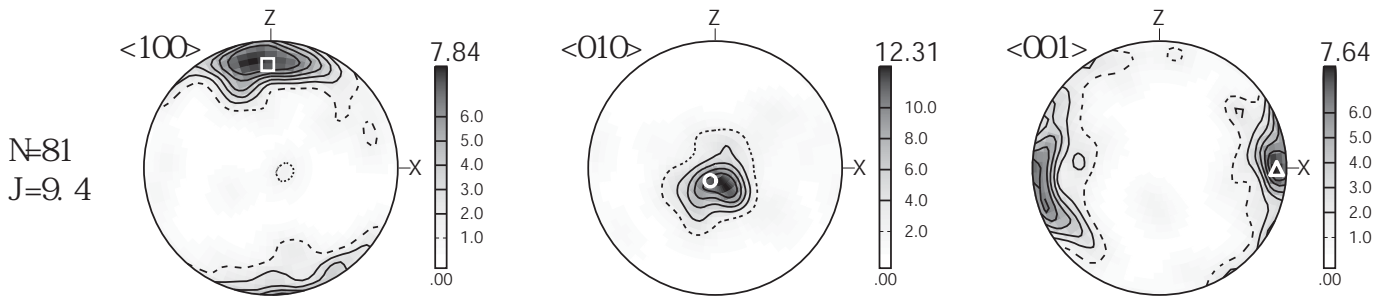




Small opx grains:
 Mean grain size: $d=44 \mu\text{m}$
 Mean aspect ratio: $r=1.54$



(B)

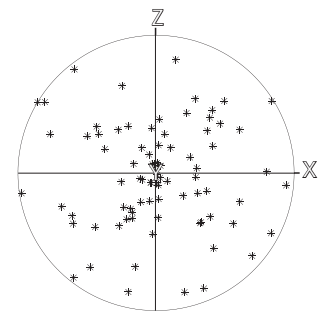


$N=81$
 $J=9.4$

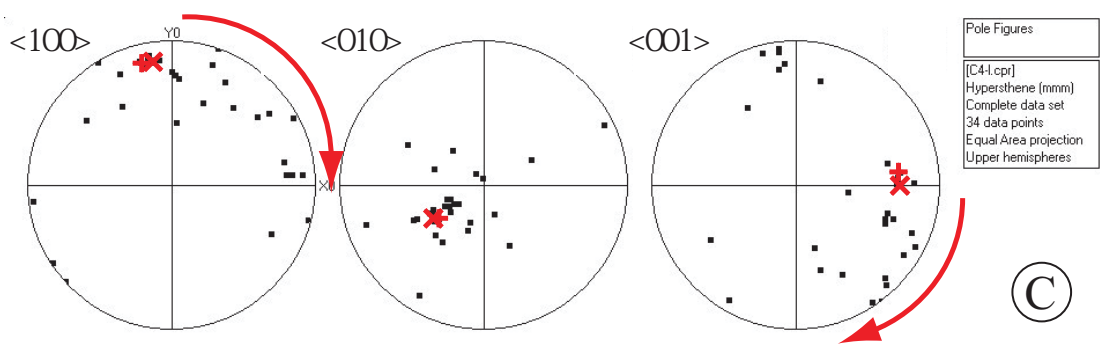
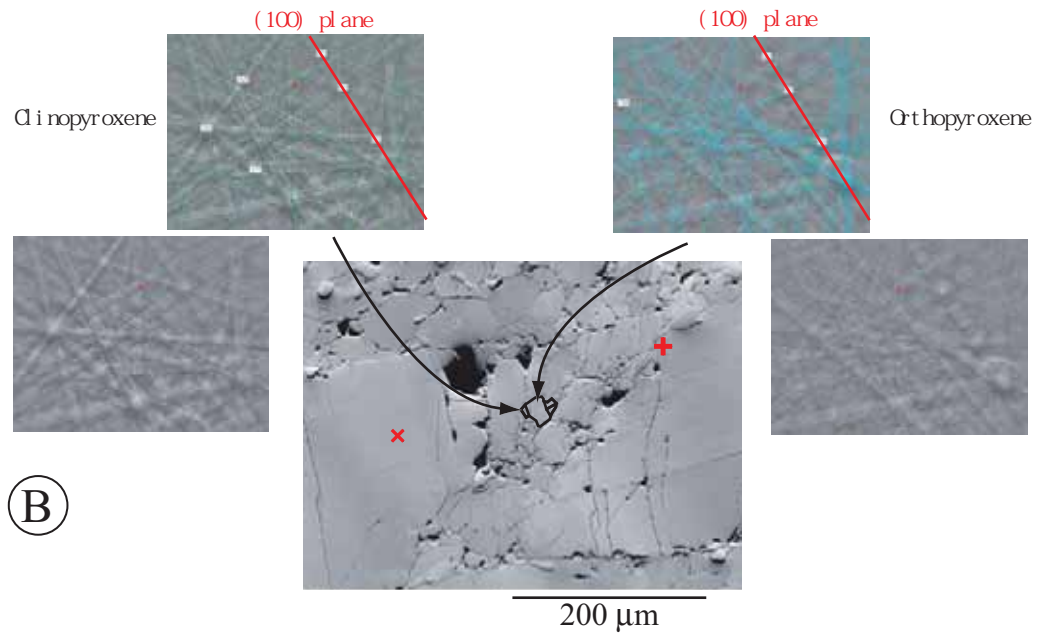
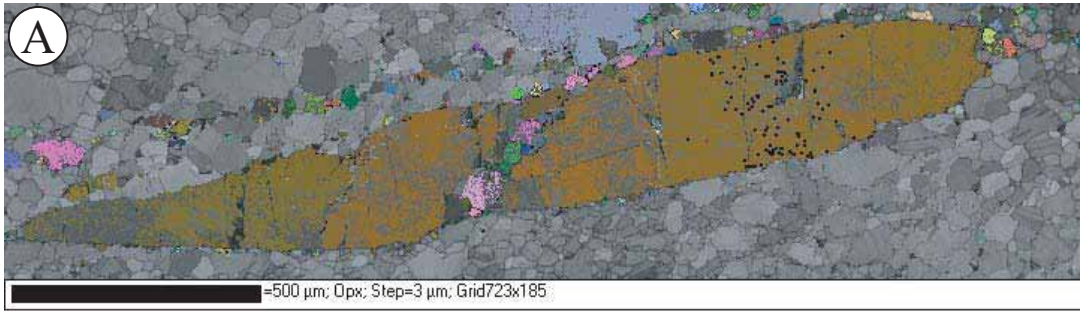
Opx porphyroclast axes

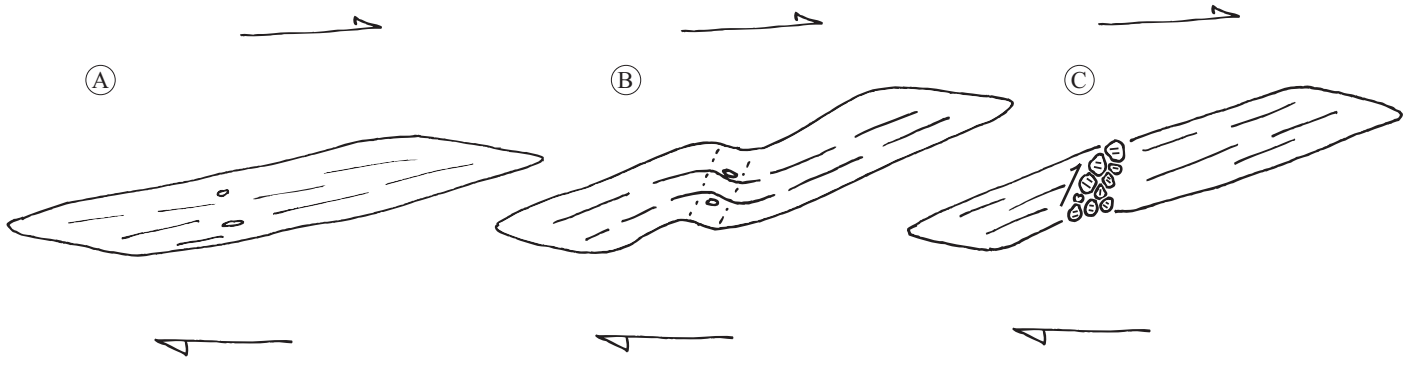
- \square $\langle 100 \rangle$ axis
- \odot $\langle 010 \rangle$ axis
- \triangle $\langle 001 \rangle$ axis

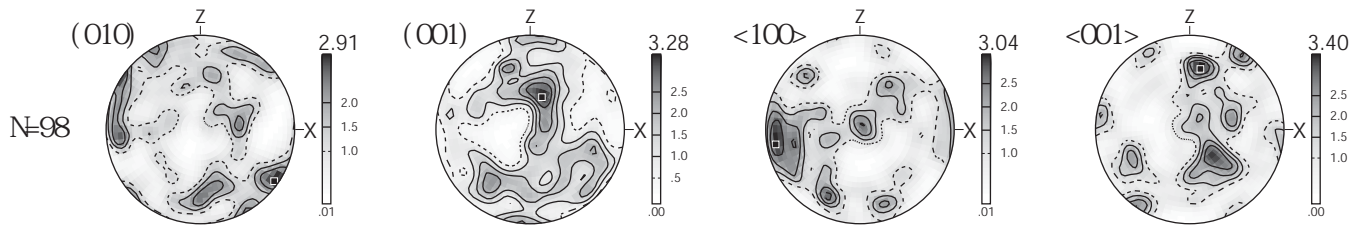
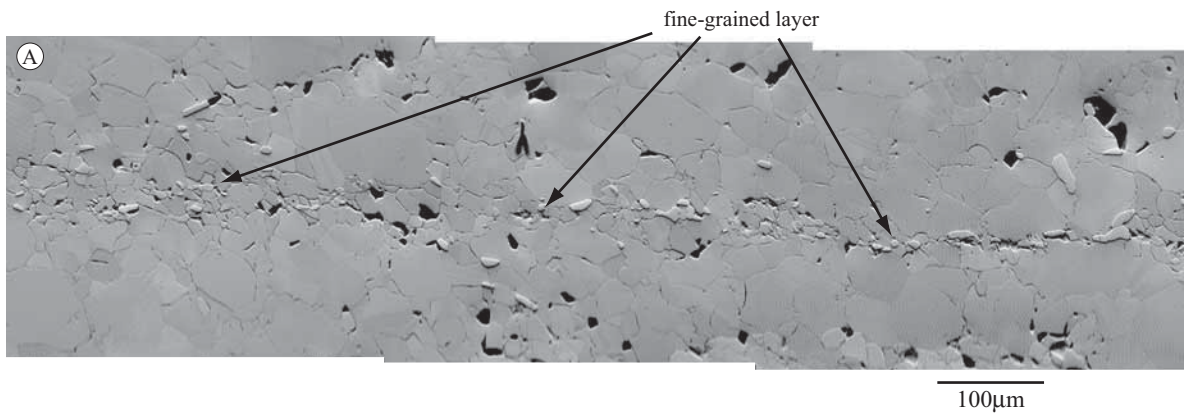
(C)



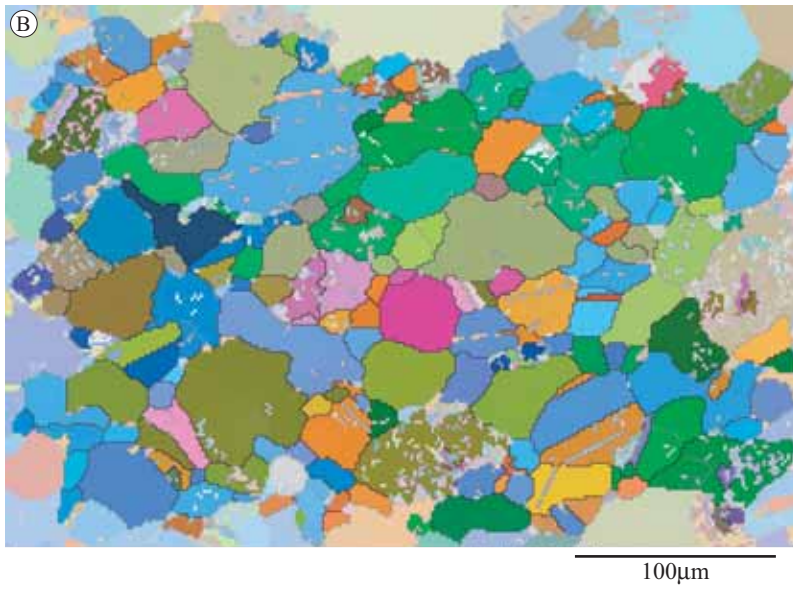
+ rotation axis



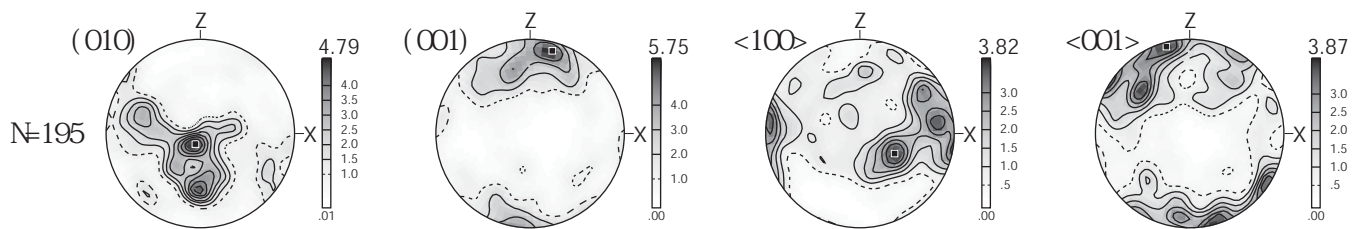


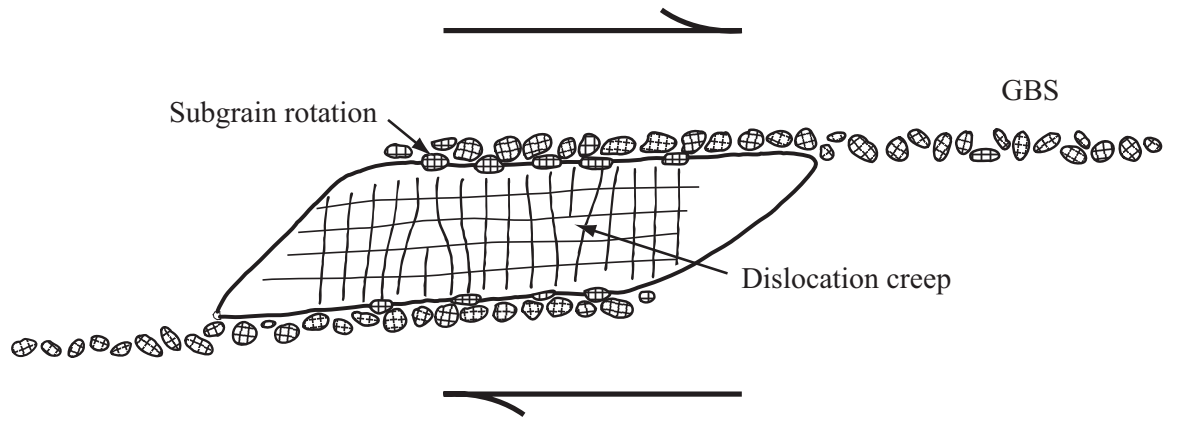


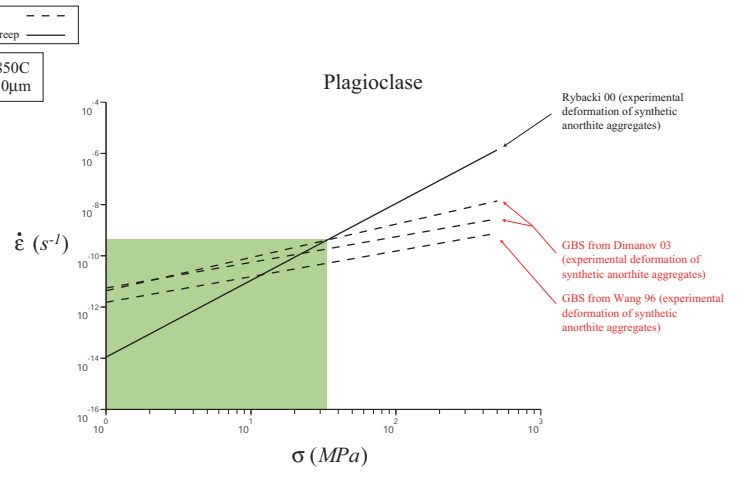
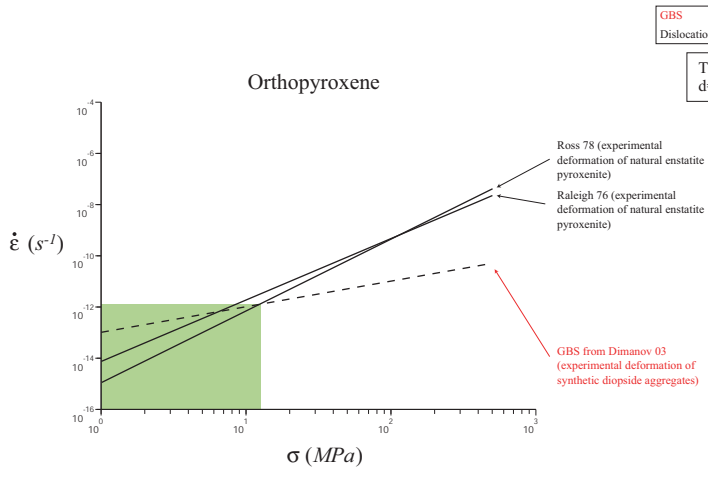
Mean grain size ~10µm



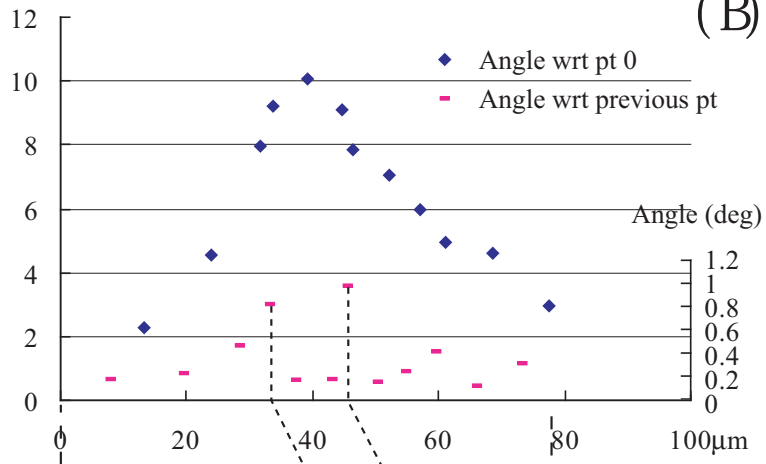
Mean grain size: $d=30\mu\text{m}$
 Mean aspect ratio: $r=1.97$



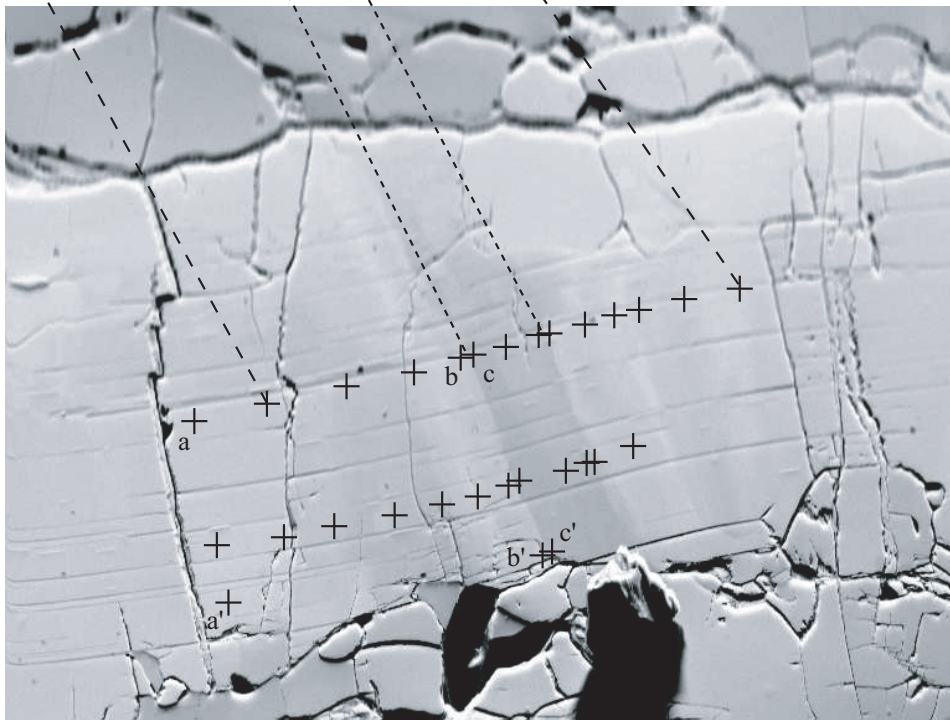




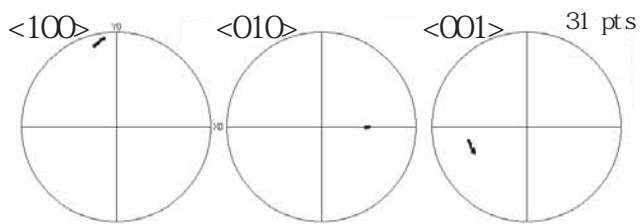
Angle (deg)



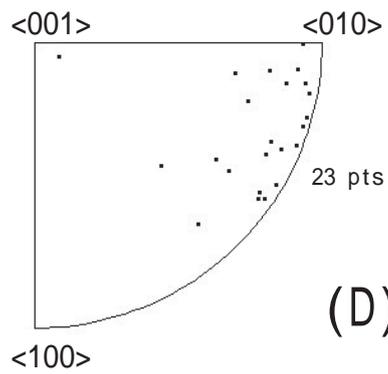
a-a': $0.82^\circ/28\mu\text{m}=2.8\cdot 10^{-2}\text{ }^\circ/\mu\text{m}$
b-b': $1.01^\circ/33\mu\text{m}=3.1\cdot 10^{-2}\text{ }^\circ/\mu\text{m}$
c-c': $0.75^\circ/33\mu\text{m}=2.3\cdot 10^{-2}\text{ }^\circ/\mu\text{m}$



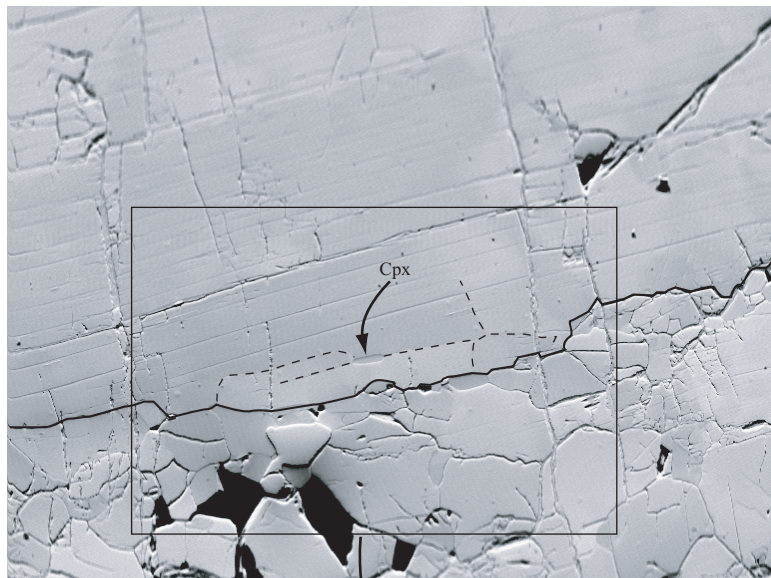
(A)



(C)



(D)



(B)



